Nanoscale Res Lett (2010) 5:478–483
DOI 10.1007/s11671-010-9545-x

SPECIAL ISSUE ARTICLE

Superelasticity of Carbon Nanocoils from Atomistic Quantum Simulations

Li Zhao Liu · Hai Li Gao · Ji Jun Zhao · Jian Ping Lu

Received: 30 August 2009 / Accepted: 16 January 2010 / Published online: 6 February 2010

Abstract A structural model of carbon nanocoils (CNCs) on the basis of carbon nanotubes (CNTs) was proposed. The Young's moduli and spring constants of CNCs were computed and compared with those of CNTs. Upon elongation and compression, CNCs exhibit superelastic properties that are manifested by the nearly invariant average bond lengths and the large maximum elastic strain limit. Analysis of bond angle distributions shows that the three-dimensional spiral structures of CNCs mainly account for their unique superelasticity.

Keywords Nanocoil · Nanotube · Superelasticity · Young's modulus

Introduction

There is a large class of novel nanostructures with helical geometries including boron carbide [1], SiC [2] and ZnO [3, 4] nanosprings, carbon [5] and ZnO [6] nanohelices, and carbon nanocoils [7, 8]. Among them, carbon nanocoil (CNC) (also known as coiled carbon nanotube) has attracted particular attention due to its structural correlation with carbon nanotubes (CNTs). Intuitively, CNCs may inherit some of the fundamental properties of carbon nanotubes but exhibit other unique mechanical, electronic, and magnetic properties associated with their coiled geometries and the intrinsic distribution of five-membered and seven-membered rings.

In early 1990s, Dunlap [9] and Ihara et al. [10–12] proposed several structural models for coiled carbon nanotubes and discussed the relationships between the geometric parameters (diameter, pitch length, rotational symmetry) and the energetic, elastic, and electronic properties. Molecular dynamics simulations and tight-binding calculations have demonstrated the structural stability of CNCs; they have higher cohesive energy ($\sim$7.4 eV/atom) than that of C_{60} (7.29 eV/atom) [10, 13]. Electronic properties of CNCs including band structures and density of states were investigated using a tight-binding model [11, 14], and it was predicted that some carbon nanocoils could be semi-metals, in contrast to the conventionally semiconducting and metallic behavior known for the straight carbon nanotubes.

Since Zhang et al. first fabricated carbon nanocoils (700 nm in pitch and $\sim$20 nm in tubular diameter) via catalytic decomposition of acetylene in 1994 [7], there have been large experimental efforts in synthesizing CNCs of high quality. Production of CNCs by chemical vapor deposition (CVD) [15–19], laser evaporation of the fullerene/Ni particle mixture [20], and opposed flow flame combustion method [21] has been reported. Pan and coworkers realized diameter control of CNCs via tuning the particle size of the nanoscale catalysts [22]. In addition to the conventionally synthesized multi-walled CNCs with tubular diameters of 15–100 nm [7, 16–19], evidence of ultrathin single-walled carbon nanocoils (with both tubular diameter and pitch length down to 1 nm) was found in the

L. Z. Liu · H. L. Gao · J. J. Zhao (✉)
Laboratory of Materials Modification by Laser, Electron, and Ion Beams, and College of Advanced Science and Technology, Dalian University of Technology, 116024 Dalian, China
e-mail: zhaojj@dlut.edu.cn

J. J. Zhao
Jiangsu Key Laboratory for Chemistry of Low-Dimensional Materials, Huaiyin Normal University, 223300 Huaian, China

J. P. Lu
Department of Physics and Astronomy, University of North Carolina at Chapel Hill, Chapel Hill, NC 27599, USA

products of carbon nanotubes from catalytic decomposition of hydrocarbon molecules by Biró's STM experiments [23].

With their unique three-dimensional (3D) helical structures, the CNCs are expected to exhibit spring-like behavior in their mechanical properties. In an experiment by Chen et al. [24], multi-walled CNCs with outer tubular diameter of ~126 nm have been elastically elongated to a maximum strain of ~42%. A spring constant of 0.12 N/m in the low strain region was obtained. According to the structural parameters of nanocoil given by Chen et al. [24] (tubular diameter of 120 nm, coil radius of 420 nm, and pitch of 2,000 nm), Fonseca et al. [25] computed the CNC's Young's modulus within the framework of the Kirchhoff rod model and obtained a value of 6.88 GPa. Using finite element analysis at the continuum level, Sanada et al. also predicted a similar result (about 4.5 GPa) for carbon nanocoil with tubular radius of 240 nm, coil radius of 325 nm, and coil pitch of 1,080 nm [26]. However, the experimentally measured Young's modulus values are much higher than these theoretical predictions. Volodin et al. [27] reported a Young's modulus ~0.7 TPa for CNCs with coil diameter >170 nm from AFM measurement. Using a manipulator-equipped SEM, Pan et al. determined the Young's modulus of CNCs to be up to 0.1 TPa for coil diameter ranging from 144 to 830 nm [28]. The large discrepancy between experiment and theory has been attributed to the usage of mechanical parameters of bulk materials in the continuum mechanics simulations [25].

Despite the above efforts, our theoretical knowledge of the CNCs is still limited. In particular, there have been no atomistic simulations of the mechanical properties of the CNCs. In this paper, we proposed a new way of constructing structural models of carbon nanocoils and computed the Young's moduli and spring constants for a series of ultrathin CNCs. Most interestingly, we observed an unusual superelasticity in these CNCs owing to their 3D spiral geometries.

Structural Model and Computational Methods

We developed a simple way to construct atomistic models for the structures of single-walled carbon nanocoils based on nanotubes with given chirality. As shown in Fig. 1, one pair of pentagons and another pair of heptagons are first individually introduced in two sides of a piece of carbon nanotube via adjusting the local topological structures of the two pairs of originally hexagonal rings (see the highlighted parts in Fig. 1a) and the surrounding carbon network. Introducing pentagons forms a cone defect, while

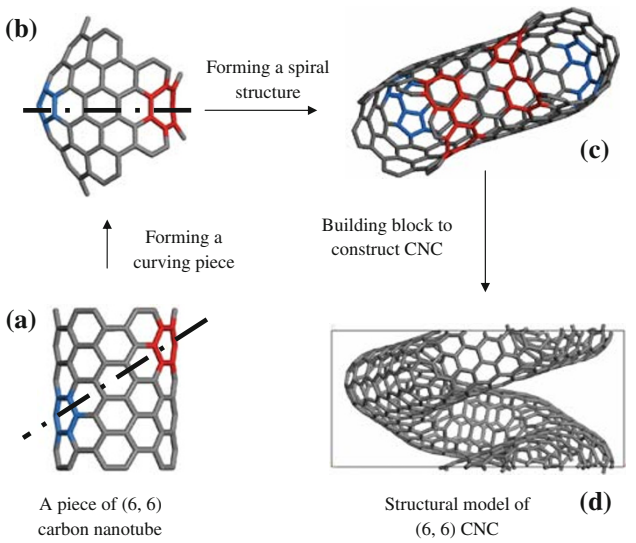

Fig. 1 (*Color online*) Procedures of constructing structural model of (6, 6) carbon nanocoil from a piece of (6, 6) carbon nanotube

introducing heptagons results in a saddle point defect (see the blue and red rings in Fig. 1b, respectively).

Upon relaxation, the nanotube segment is bent around the defect site in order to release the strain energy induced by the pentagons and heptagons. The pentagon (heptagon) pair locates in the convex (concave) part of the segment (see Fig. 1b), passing through a bisector after we adjust the number of carbon atoms on the two ends to make the segment symmetric. Depending on how these basic structural segments are connected, either a nanocoil or a nanotori [9, 29, 30] is formed. As shown in Fig. 1c, two segments are connected with a certain rotating angle to make the combined structure spiral and to form a seamless hexagonal carbon network.

The structure in Fig. 1c can be further used as a building block to construct complete nanocoils with one-dimensional (1D) periodic boundary conditions (see Fig. 1d). By changing the tube length at the two ends of the basic segment (Fig. 1b) or varying the nanotube diameter, we can control coil diameter, coil pitch, and tubular diameter of a carbon nanocoil. In such a way, we built a series of single-walled carbon nanocoils, that is, (5, 5), (6, 6), (7, 7), and (8, 8) CNCs. Here, the index (n, n) for a CNC means that the CNC is constructed from the straight (n, n) nanotube. As shown in Fig. 2, a typical nanocoil exhibits a polygonal shape from the top view, in coincidence with experimental observation [31]. The effective coil diameter d of a nanocoil is nearly proportional to its tubular diameter as well as the side length of the basic segment (see Table 2); but there is no simple relationship between the coil pitch and the other geometry parameters. At present, for a given nanotube, we chose to construct nanocoils using the building blocks with the smallest side length

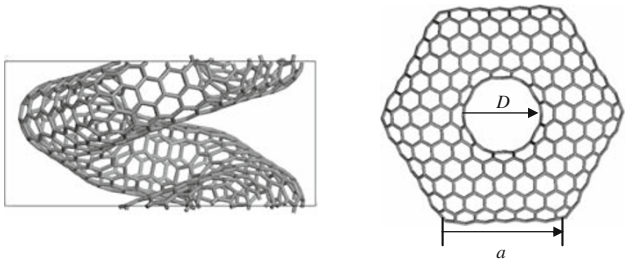

Fig. 2 Geometry of (6, 6) CNC from *side view* (*left plot*) and *top view* (right plot); the *latter* is a hexagonal nanotori. a is the side length of hexagon, D is the diameter of the inner ring. The area of cross section (from *top view*) is computed by $S = 3\sqrt{3}a^2/2 - \pi(D/2)^2$

(corresponding to the length of the straight nanotube on each basic segment).

The structures and energetics of these CNCs were described by a nonorthogonal tight-binding (TB) model developed by our group previously [32]. This TB total energy model is based on the extended Hückel approximation and employed an exponential distance-dependent function for the hopping integral overlap. The TB parameters were especially developed for hydrocarbon molecules and nanostructures. The experimental or ab initio data on the geometry structures, binding energies, on-site charge transfer, and vibrational frequencies of a variety of hydrocarbon molecules have been well reproduced. In addition, a few test calculations on the carbon fullerenes and nanotubes also showed satisfactory agreement between TB and DFT results.

Within 1D periodic boundary condition, the lattice parameter (pitch) of each nanocoil was carefully adjusted to minimize the total energy. Starting from the equilibrium 1D lattice, the CNCs were either compressed or elongated by gradually varying the lattice parameter to investigate the mechanical properties of these nanocoils. At any given lattice parameter, the atomic coordinates of CNCs were fully relaxed without any symmetry constraint. To validate the results from TB calculations, we performed all-electron density functional theory (DFT) calculations on the smaller (5, 5) CNC. In the DFT calculations, we adopted generalized gradient approximation (GGA) with the PW91 parameterization [33] and the double-numerical plus d polarization (DND) basis set as implemented in the DMol^3 package [34].

Results and Discussion

Young's Modulus and Spring Constant

The mechanical properties of a carbon nanocoil can be characterized by spring constant (k) and Young's modulus (E), which can be computed by the following two formula:

$$U = \frac{1}{2}kx^2, \tag{1}$$

$$E = \frac{1}{V_0}.\frac{\partial^2 U}{\partial \varepsilon^2}, \tag{2}$$

where U is the elastic potential energy of the system (total energies differences of different lengths), $x = |L - L_0|$ and $\varepsilon = |L - L_0|/L_0$ are the 1D displacement and strain under elongation/compression, respectively, L is the length of 1D unit cell and the L_0 is its equilibrium value, and V_0 is the effective volume of the 1D structural unit in its equilibrium configuration. For a carbon nanocoil, $V_0 = S \times L_0$, where S is the area of cross section of the nanocoil from the top view (see Fig. 2). Similarly, for a single-walled carbon nanotube, $V_0 = 2\pi r \times L_0 \times \Delta d$, where $\Delta d = 3.4$ Å is the shell thickness of tube wall and r is the tube radius [35, 36].

Using DFT results as benchmark, we first calculated the Young's modulus of a series of armchair carbon nanotubes to assess the validity of the present TB total energy model. Starting from the equilibrium 1D lattice length, we elongated different armchair CNTs along the axis direction with a strain step of 0.2% up to a maximum strain of 1%. The computational 1D supercells of 29.54 Å in length include 12 unit cells of nanotube. The theoretical Young's moduli of CNTs from DFT and TB calculations are listed in Table 1. Both methods predicted that the Young's moduli of CNTs are around 1.0 TPa, nearly independent of tube diameter. Similar results were obtained in previous theoretical [36] and experimental [37] studies on CNTs. The agreement between the TB and DFT calculations and the coincidence with previous results indicate that the present TB model should be reasonable for describing the mechanical properties of carbon nanostructures.

Similarly, the Young's moduli and spring constants of CNCs were calculated via stretching the system along the orientation of their spiral axis. Within a maximum strain of 5%, we gradually applied the elongation strain by a step of 1%. The Young's moduli of CNCs from TB calculations are listed in Table 2. For all systems studied, the computed Young's moduli range between three and six GPa. For the smallest (5, 5) nanocoil considered, our DFT calculations yield a Young's modulus of $E = 5.31$ GPa, rather close to

Table 1 Young's modulus (E) of different armchair carbon nanotubes from DFT (E_{DFT}) and TB (E_{TB}) calculations

Nanotube	r (Å)	E_{DFT} (GPa)	E_{TB} (GPa)
(5,5)	3.40	969.7	983.4
(6,6)	4.08	929.1	984.7
(7,7)	4.76	941.6	986.0
(8,8)	5.44	962.3	989.9

r is the tube radius

Table 2 Young's modulus (E) and spring constant (k) of carbon nanocoils (CNCs) from TB and DFT (values in brackets) calculations

Nanocoil	L_0 (Å)	S (Å^2)	d (Å)	E (GPa)	k (N/m)
(5,5)	13.61	369.79	26.38	5.40 (5.31)	15.37 (15.54)
(6,6)	12.64	470.54	28.85	4.49	16.65
(7,7)	12.11	662.10	33.58	3.43	18.66
(8,8)	12.27	924.98	39.21	4.52	44.36

L_0 is the equilibrium pitch length of CNC in the spiral direction; S is the area of cross section from top view, d is the effective coil diameter

the TB value (5.4 GPa). Compared with those of carbon nanotubes, the Young's moduli of nanocoils are lower by two orders of magnitude, indicating that the CNCs are quite soft with regard to CNTs owing to their unique spring-like geometry. The Young's moduli for the ultrathin nanocoils from our present atomistic calculations are comparable to those of previous theoretical results for mesoscale nanocoils. Unfortunately, there are no experimental data reported for ultrathin CNCs with diameters down to several nanometers.

Although the computed Young's modulus for nanocoil varies with the tubular diameter and coil diameter (see Table 2), there seems no clear diameter-dependent trend, in agreement with the experimental observations [27, 28]. For carbon nanocoils of diameters between 144 and 830 nm, Hayashida et al. [28] found that the Young's modulus changes irregularly from 0.04 TPa to 0.10 TPa. Volodin's measurement of Young's modulus also revealed no apparent dependence on the coil diameter [27].

The spring constants of the CNCs were also computed using Eq. (1), and the results are listed in Table 2. For the (5, 5), (6, 6), and (7, 7) CNCs, the spring constants are around 15–19 N/m, whereas the (8, 8) CNC possesses a very large spring constant of 44.36 N/m. Previous experiment by Chen et al. [24] obtained a $k = 0.12$ N/m for a mesoscale CNC (tubular diameter of 120 nm, coil radius of 420 nm, and pitch of 120 nm). The discrepancy between the present theoretical values and the measured data might be understood by the different length scales of the systems (nanometers in our model systems versus hundreds of nanometers in experimental CNCs).

Superelasticity

For macroscopic materials, the superelastic (or pseudoelastic) effect in the shape memory alloys results in a variety of useful industrial and medical applications [38]. In the nanostructured materials, similar superelastic phenomena were recently revealed in nanocoils and microcoils. Gao et al. reported superelasticity in ZnO nanohelices ($\sim$560 nm in coil diameter) with an experimental maximum elongation of 69.8% measured by AFM and a theoretical maximum elongation of 72% calculated by classical elasticity theory [6]. A Si_4N_3 microcoil with coil diameter of 160 μm also exhibited good recovery ability under repeated load, corresponding to the superelasticity [39]. In particular, even when stretched to a nearly straight shape for several cycles, the Si_4N_3 microcoil recovered its original state without damage after the load was released. As for the coiled carbon structures, Motojima et al. revealed that carbon microcoils could be extended and contracted by 3–15 times [40] and 5–10 times [41] with regard to the original coil length. Meanwhile, carbon nanocoils also demonstrated superior elasticity with a maximum relative elongation of $\sim$42% [24].

In this work, we applied elongation (compressive) strains up to about 60% (20–35%) on different CNCs. Above such elastic limits, the CNCs will undergo plastic deformation, which will not be discussed here. Within the elastic strain ranges considered, the CNCs hold their topological structures very well upon geometry relaxation. We further examined the changes of average C–C bond lengths of CNCs during elongation and compression. As shown in Fig. 3, the average C–C bond length is very robust under external strains of both directions. With elongation strain up to 50%, the increase in average bond length is only less than 0.6% for (5, 5), 0.4% for (6, 6), and 0.3% for (7, 7) CNC, respectively. On the other hand, the average C–C bond length is slightly reduced under 1D compression. For a (5, 5) CNC, the magnitude of average bond length reduction is about 0.4% up to a maximum compressive strain of 35%. In additional to the above TB results, DFT calculations were carried out on the (5, 5) CNC to further confirm the change of average bond length during elongation and compression. As shown in the insert

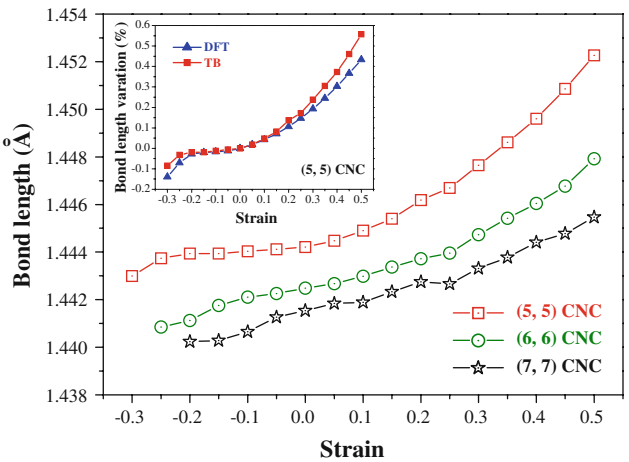

Fig. 3 Variation of average C–C bond length in carbon nanocoils (CNCs) under elongation (positive) and compressive (negative) strains. The *insert plot* shows the comparison of percentages of bond length variation with regard to the equilibrium state for a (5, 5) CNC from DFT and TB calculations

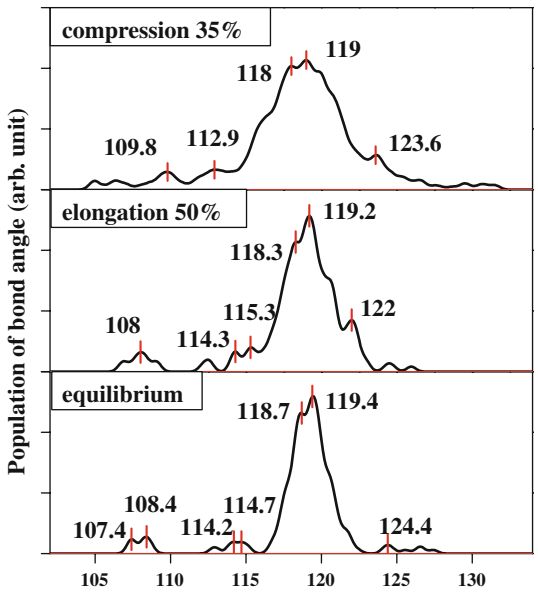

Fig. 4 Bond angle distribution of (5, 5) carbon nanocoil under large elongation (50%) and compressive strain (35%), compared to the equilibrium case

plot of Fig. 3, up to an elongation strain of 50% (a compressive strain of 30%), the increase (decrease) in average bond length is 0.5% (0.14%) from DFT calculations, comparable to the TB values of 0.6% (0.08%). The excellent coincidence between DFT and TB results proves that the present TB model is reliable at least for describing the elastic properties of the carbon nanocoils.

With increasing tubular diameter, the variation of average bond length in the nanocoil is less sensitive to elongation strain (see Fig. 3), implying that the nanocoil can undertake higher strain. On the contrary, the elastic limit of compression for a CNC reduces with increasing tubular diameter. For example, the maximum compressive strain is 35% for (5, 5) CNC, 25% for (6, 6) CNC, and 20% for (7, 7) CNC. It is interesting to note that the carbon nanocoils can undertake higher elongation strain (up to ~60%) than compressive one (up to 20–35%).

The above computational results show superior superelasticity in CNCs. In particular, under elongation strain up to 60%, the topology structure of the carbon nanocoil is still retained, with an average bond length only increased by less than 1%. This phenomenon can be partially understood by the 3D spiral structures of the CNCs, which offer enough flexibility to be stretched or squeezed. Due to the substantial strength of C–C bond (with average bond energy over 2 eV), the relative orientations of neighboring C–C bonds (i.e., bond angles) in a nanocoil would alter during compression or elongation in order to avoid significant changes of C–C bond lengths. As shown in Fig. 4, the full width at half maximum (FWHM) of bond angle distribution for a (5, 5) CNC increases during elongation or compression. For example, the FWHM for the equilibrium (5, 5) CNC is 2.7°. It increases to 3.5° under an elongation strain of 50%, and 5.6° for a compressive strain of 35%. The superelastic behavior predicted for CNCs may lead to some applications in nanoscale materials and devices, for example, shape memory, elastic energy storage, buffer, nano-spring in NEMS, and so on.

Conclusion

We have constructed a series of carbon nanocoils by periodically introducing pentagons and heptagons in the segments of carbon nanotubes to make them coiled. The computed Young's moduli of carbon nanocoils (3–6 GPa) are much lower than those of carbon nanotubes (~1 TPa). Under large elongation/compressive strains, the average bond lengths of CNCs almost remain invariant, while the elastic energy is stored via bond angle redistributions, corresponding to the superelastic behavior. Compared to the carbon nanotubes with same chirality, nanocoils show much smaller Young's moduli and unusual superelasticity, which might lead to some future nanotechnology applications.

Acknowledgments This work is supported by NCET Program provided by the Ministry of Education of China (NCET-060281), and the Scientific Research Foundation for the Returned Overseas Chinese Scholars.

References

1. D.N. McIlroy, D. Zhang, Y. Kranov, M.G. Norton, Appl. Phys. Lett. **79**, 1540 (2001). doi:10.1063/1.1400079
2. D. Zhang, A. Alkhateeb, H. Han, H. Mahmood, D.N. McIlroy, M.G. Norton, Nano Lett. **3**, 983 (2003). doi:10.1021/nl034288c
3. X.Y. Kong, Z.L. Wang, Nano Lett. **3**, 1625 (2003). doi:10.1021/nl034463p
4. P.X. Gao, Z.L. Wang, Small **1**, 945 (2005). doi:10.1002/smll.200500165
5. G. Zhang, X. Jiang, E. Wang, Appl. Phys. Lett. **84**, 2646 (2004). doi:10.1063/1.1695198
6. P.X. Gao, W.J. Mai, Z.L. Wang, Nano Lett. **6**, 2536 (2006). doi:10.1021/nl061943i
7. X.B. Zhang, X.F. Zhang, D. Bernaerts, G.T. Vantendeloo, S. Amelinckx, J. Vanlanduyt, V. Ivanov, J.B. Nagy, P. Lambin, A.A. Lucas, Europhys. Lett. **27**, 141 (1994). doi:10.1209/0295-5075/27/2/011
8. L. Kin Tak, L. Mei, H. David, Compos. Part. B. Eng. **37**, 437 (2006). doi:10.1016/j.compositesb.2006.02.008
9. B.I. Dunlap, Phys. Rev. B **46**, 1933 (1992). doi:10.1103/PhysRevB.46.1933

10. S. Ihara, S. Itoh, J.-I. Kitakami, Phys. Rev. B **48**, 5643 (1993). doi:10.1103/PhysRevB.48.5643
11. K. Akagi, R. Tamura, M. Tsukada, S. Itoh, S. Ihara, Phys. Rev. Lett. **74**, 2307 (1995). doi:10.1103/PhysRevLett.74.2307
12. S. Ihara, S. Itoh, Carbon **33**, 931 (1995). doi:10.1016/0008-6223(95)00022-6
13. O.Y. ZhongCan, Z.B. Su, C.L. Wang, Phys. Rev. Lett. **78**, 4055 (1997). doi:10.1103/PhysRevLett.78.4055
14. K. Akagi, R. Tamura, M. Tsukada, S. Itoh, S. Ihara, Phys. Rev. B **53**, 2114 (1996). doi:10.1103/PhysRevB.53.2114
15. L.J. Pan, T. Hayashida, M. Zhang, Y. Nakayama, Jpn. J. Appl. Phys. Pt. 2 Lett. **40**, L235 (2001). doi:10.1143/JJAP.40.L235
16. D. Pradhan, M. Sharon, Mater. Sci. Eng. B **96**, 24 (2002). doi:10.1016/S0921-5107(02)00309-4
17. S. Takenaka, M. Ishida, M. Serizawa, E. Tanabe, K. Otsuka, J. Phys. Chem. B **108**, 11464 (2004). doi:10.1021/jp048827t
18. J.N. Xie, K. Mukhopadyay, J. Yadev, V.K. Varadan, Smart Mater. Struct. **12**, 744 (2003). doi:10.1088/0964-1726/12/5/010
19. L.J. Pan, M. Zhang, Y. Nakayama, J. Appl. Phys. **91**, 10058 (2002). doi:10.1063/1.1471575
20. A.A. Koos, R. Ehlich, Z.E. Horvath, Z. Osvath, J. Gyulai, J.B. Nagy, L.P. Biró, Mater. Sci. Eng. C **23**, 275 (2002). doi:10.1016/S0928-4931(02)00255-2
21. A.V. Saveliev, W. Merchan-Merchan, L.A. Kennedy, Combust. Flame **135**, 27 (2003). doi:10.1016/S0010-2180(03)00142-1
22. S. Hokushin, L. Pan, Y. Nakayama, Jpn. J. Appl. Phys. **46**, 5383 (2007). doi:10.1143/JJAP.46.5383
23. L.P. Biró, S.D. Lazarescu, P.A. Thiry, A. Fonseca, J.B. Nagy, A.A. Lucas, P. Lambin, Europhys. Lett. **50**, 494 (2000). doi:10.1209/epl/i2000-00296-0
24. X.Q. Chen, S.L. Zhang, D.A. Dikin, W.Q. Ding, R.S. Ruoff, L.J. Pan, Y. Nakayama, Nano Lett. **3**, 1299 (2003). doi:10.1021/nl034367o
25. A.F. da Fonseca, C.P. Malta, D.S. Galvao, Nanotechnology **17**, 5620 (2006). doi:10.1088/0957-4484/17/22/015
26. K. Sanada, Y. Takada, S. Yamamoto, Y. Shindo, J. Solid Mech. Mater. Eng. **2**, 1517 (2008). doi:10.1299/jmmp.2.1517
27. A. Volodin, M. Ahlskog, E. Seynaeve, C. Van Haesendonck, A. Fonseca, J.B. Nagy, Phys. Rev. Lett. **84**, 3342 (2000). doi:10.1103/PhysRevLett.84.3342
28. T. Hayashida, L. Pan, Y. Nakayama, Physica B **323**, 352 (2002). doi:10.1016/S0921-4526(02)01002-5
29. S. Ihara, S. Itoh, J.-I. Kitakami, Phys. Rev. B **47**, 12908 (1993). doi:10.1103/PhysRevB.47.12908
30. S. Itoh, S. Ihara, J.-I. Kitakami, Phys. Rev. B **47**, 1703 (1993). doi:10.1103/PhysRevB.47.1703
31. X.F. Zhang, Z. Zhang, Phys. Rev. B **52**, 5313 (1995). doi:10.1103/PhysRevB.52.5313
32. J. Zhao, X. Guo, B. Wen, Mol. Simulat. **33**, 703 (2007). doi:10.1080/08927020701203706
33. J.P. Perdew, Y. Wang, Phys. Rev. B **45**, 13244 (1992). doi:10.1103/PhysRevB.45.13244
34. B. Delley, J. Chem. Phys. **92**, 508 (1990). doi:10.1063/1.458452
35. E. Hernandez, C. Goze, P. Bernier, A. Rubio, Phys. Rev. Lett. **80**, 4502 (1998). doi:10.1103/PhysRevLett.80.4502
36. J.P. Lu, Phys. Rev. Lett. **79**, 1297 (1997). doi:10.1103/PhysRevLett.79.1297
37. E.W. Wong, P.E. Sheehan, C.M. Lieber, Science **277**, 1971 (1997). doi:10.1126/science.277.5334.1971
38. D.C. Lagoudas, *Shape memory alloys: modeling and engineering applications* (Springer, Berlin, 2008)
39. C.B. Cao, H.L. Du, Y.J. Xu, H.S. Zhu, T.H. Zhang, R. Yang, Adv. Mater. **20**, 1738 (2008). doi:10.1002/adma.200701021
40. S. Motojima, X. Chen, S. Yang, M. Hasegawa, Diam. Relat. Mater. **13**, 1989 (2004). doi:10.1016/j.diamond.2004.06.020
41. S.M. Yang, X.Q. Chen, H. Aoki, S. Motojima, Smart Mater. Struct. **15**, 687 (2006). doi:10.1088/0964-1726/15/3/003